Available online at www.sciencedirect.com

SciVerse ScienceDirect

Procedia Engineering 48 (2012) 469 – 478

Procedia Engineering

www.elsevier.com/locate/procedia

MMaMS 2012

Simple electro-mechanical model of magnetic spring realized from FeNdB permanent magnets

Miroslav Novak[a], Josef Cernohorsky[a], Miloslav Kosek[a]*

[a]*Technical University of Liberec, Sudentska 2, 46117 Liberec 1, Czech Republic*

Abstract

Magnetic spring utilizing the repulsive force of two permanent magnets is a new device with application in special textile machines. In order to get reliable rules for its design, the effect of geometrical parameters, magnetic properties, material deviations and mechanical inaccuracies should be known, first of all. The paper presents very simple model of permanent magnets based on surface bounded currents and gives information from detailed measurement of ring shape magnet both of the magnetic field and repulsive force. At present time the magnetic field measurement was performed only in a plane parallel to the spring plane. Nevertheless, the agreement with theory is good and the experimental errors can be estimated and reduced by the method of trials and errors. The value of magnetic flux density agrees with the producer data and its deviation can reach up to 10 % along the concentric circle. Also, the direct measurement of repulsive force agrees well with both the simple theory and two-dimensional FEM. Ring magnet with outer diameter of 25 mm exhibits magnetic flux density of 1.15 T on its surface and a repulsive force of about 70 N in close contact between magnets. The dynamic magnet aging was studied, too. The changes in both the magnetic field and repulsive force were negligible after 30 million cycles. After finishing the experiments, the method and all the results can make very efficient and simple design of magnetic spring.

Keywords: Bounded magnetic currents; Ring parmanent magnets; Repulsive magnetic force; Magnet dynamic aging; Precise measurement of magnetic flux density

Nomenclature

d	inner magnet diameter (m)
D	outer magnet diameter (m)
h	magnet height (m)
$\mathbf{B}_r$	magnetic flux density on the magnet surface (T)
$\mathbf{M}$	magnetization (A/m)
Greek symbols	
μ_0	permeability of vacuum
Subscripts	
b	bounded current

* Corresponding author.
E-mail address: miloslav.kosek@tul.cz

doi:10.1016/j.proeng.2012.09.541

1. Introduction

Modern permanent magnets of FeNdB composition are used in many technical areas because of their high magnetic field. One of new application is their use as magnetic springs that utilize their repulsive magnetic force. Probably a ring shape magnet is the best solution for our purpose of magnetic spring in textile spinning machine. The repulsive force depends on the magnetic properties of material and the ring shape, its inner diameter d, outer diameter D and height h. As for magnetic properties the producers defines magnetic flux density B_r on its surface. It is a constant parameter, while the geometrical parameters can be changed. In general, in the case of magnetic spring synthesis, the goal of the design is to find the optimum magnet geometry for the given repulsive force at given mutual position of magnets, usually in close contact. It is evident that there is a lot of solutions, therefore other limitation are necessary. Usually the ranges of ring dimensions are given.

The opposite task, spring analysis, calculates the repulsive force for magnets of given geometrical parameters as a function of their distance. In order to calculate the force, magnetic fields of both the magnets must be known. Therefore, the magnetic field calculation is the key part of the task. Irrespective of comparatively simple magnet shape, the analytical formula exists only for the points on the magnet main axis of symmetry. In other points the solution must be found numerically. Favorite approach is to use the FEM (Finite Element Method). An alternative approach uses the integral equations that we use here. We have not found in the literature that this problem had been solved by such a way.

From the technical point of view the spring realization is influenced by the production inaccuracies both material and geometrical ones. The theme is discussed in the literature on magnets, for instance [1-2]. It is the subject of extensive experiments.

In machine application the dynamic magnet aging plays an important role. The dynamic aging is the decreases of the magnetic properties with time. The reason is a very small, but repeated, demagnetization, if magnets are close one another. The theme is also treated in literature, for instance [3-4]. It is not main subject of the paper.

Main part of the paper deals with analysis of magnetic spring. Very simple model of surface bounded current is created in theoretical part. Spatial magnetic field is calculated numerically from surface bounded currents by the use of Biot Savart Law. The magnetic force is calculated from Lorentz Force Law using magnetic flux density from one magnet and surface bounded current for the other magnet.

The model must be verified experimentally. Apparatus for automated precise measurement of magnetic flux density is described and a simple mean for the measurement of the repulsive force is mentioned. The curves derived from model are compared with experimental points and the difference is analyzed and discussed.

2. Theory

The theory consists of two parts. First of all the magnetic field must be calculated. Then the magnetic force can be derived. As for the magnetic field, in principle, there are two basic procedures for the computation of magnetic field: the differential and integral ones. The differential approach is used in the well-known FEM calculations. Here we use the integral approach for its some advantages. In this case there are two basic possibilities

- Elementary magnetic dipoles.
- Bounded surface and volume currents.

Irrespective of used method, permanent magnets are described by magnetization **M,** which is defined as a magnetic momentum of unit volume of uniform material. Therefore, the elementary volume dV exhibits an elementary magnetic momentum

$$\mathrm{d}\mathbf{m} = \mathbf{M}(\mathbf{r}_0)\,\mathrm{d}V. \tag{1}$$

This Equation (1) has two meanings. First of all, it explains the definition of magnetization, which is in general function of position vector $\boldsymbol{r}_0$, and, the second, it can be used in the well-known formula for the calculation of magnetic flux density of elementary magnetic dipole of momentum d**m**. However, we will not go by this way. We will use an alternative approach of bounded currents.

Specific notation in Eq. (1) and following formulae or equations is used for position vectors. Vector $\mathbf{r}_0$ shows the position of magnetization, which is material parameter. Therefore, the term material vector is used for this vector. Vector **r** defines position of the vector of magnetic flux density, which is a field; therefore, it is a field vector.

2.1. Bounded currents

The textbooks on electromagnetic field show that the effect of elementary magnetic dipoles is equivalent to the bounded currents that flow both on the surface and in the volume of magnetized media, in general. For the density of bounded volume currents the following equation is valid

$$\mathbf{i}_b(\mathbf{r}_0) = \text{rot } \mathbf{M}(\mathbf{r}_0) = \text{curl } \mathbf{M}(\mathbf{r}_0). \quad (2)$$

The spatial derivations in the vector analytical operation rot (or curl in another notation) are made by the material coordinates, which is symbolically denoted by material position vector $\mathbf{r}_0$. The bounded surface currents have the density

$$\mathbf{j}_b(\boldsymbol{r}_0) = \text{Rot } \mathbf{M}(\mathbf{r}_0) = \mathbf{n} \times (\mathbf{M}_2(\mathbf{r}_0) - \mathbf{M}_1(\mathbf{r}_0)) = -\mathbf{n} \times \mathbf{M}(\mathbf{r}_0), \quad (3)$$

where **n** is the surface normal from the magnetic body (index 1) to vacuum (index 2). The symbol x is used for vector product and symbol Rot means the area rotation. In vacuum the magnetization is zero, $\mathbf{M}_2(\mathbf{r}_0)=0$. Therefore, in the body $\mathbf{M}_1(\mathbf{r}_0)=\mathbf{M}(\mathbf{r}_0)$. Strictly speaking, the material vector $\boldsymbol{r}_0$ should not be used outside the body, for magnetization $\mathbf{M}_2(\mathbf{r}_0)$.

The used ring magnet was polarized in the direction of its thickness along its axial symmetry, see axis *Z* in Fig. 1. In this practical case we have made the basic assumption that the magnetization is uniform. Unfortunately, the supplier data sheet does not deal with magnetization distribution. It contains only one value of permanent flux density, more correctly, its low and high limits. This assumption is not valid exactly, since the magnetization is strictly uniform only in an ellipsoid. Therefore, the uniform magnetization can be supposed with small errors, if the ring magnet cross-section is circle or ellipse. In the case of rectangular cross-section, as in our case in Fig. 1, the magnetization will not be uniform at least near the edges. Nevertheless the assumption is useful and practical, see part Results.

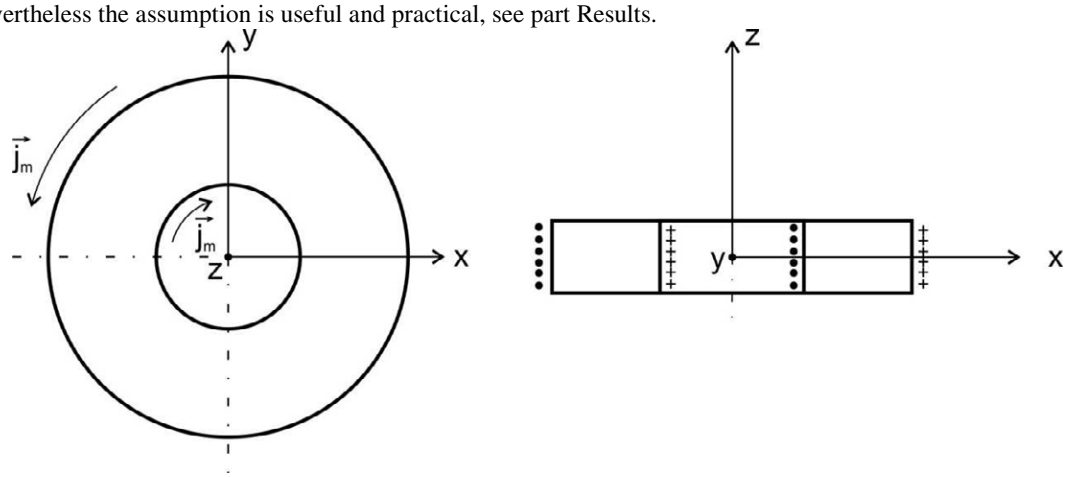

Fig. 1. Bounded surface currents of ring shape permanent magnet. Left hand part is for the plane normal to axial symmetry (axis *Z*), right hand part shows the cross section parallel to the *Z* axis.

For supposed uniform magnetization no volume bounded currents are present, as a result of Eq. (2), and the surface bounded current density is uniform, Eq. (3). The surface currents flow on the circular surfaces of ring magnets in opposite directions as it is schematically shown by dots and crosses in right hand part of Fig. 1. Total two types surface currents of opposite direction and constant density are on outer and inner vertical face of magnet surface.

Since only the value of permanent flux density $\boldsymbol{B}_r$ is known from producer, the magnetization $\boldsymbol{M}$ must be calculated from material equation

$$\mathbf{B}_r = \mu_0 (\mathbf{H}+\mathbf{M}), \quad (4)$$

where $\mu_0 = 4\pi.10^{-7}$ H/m is permeability of vacuum. As no free currents are present, **H**=0, and we get a simple formula for magnetization and bounded surface current from the material equation (4) and definition in Eq. (3)

$$j_b = M = B_r / \mu_0. \quad (5)$$

Since both the magnetization and bounded surface current has only one value, vectors are omitted in Eq. (5). Absolute value of bounded surface current is in Eq. (5).

2.2. Magnetic field and force

As soon as both the surface and volume current densities are given, the magnetic field flux density can be calculated by the use of Biot-Savart Law. Bounded volume currents produce the field.

$$\mathbf{B}(\mathbf{r}) = \frac{\mu_0}{4\pi}\int_{(V)} \frac{\mathbf{i}_b(\mathbf{r}_0)\times(\mathbf{r}-\mathbf{r}_0)}{|\mathbf{r}-\mathbf{r}_0|^3}\,\mathrm{d}V_0 \tag{6}$$

where symbol (V) is us used for the volume of permanent magnet. The magnetic flux density $\mathbf{B}(\mathbf{r})$ is calculated in the point given by the field position vector $\mathbf{r}$, while the material position vector $\mathbf{r}_0$ defines the point of exciting elementary current $\mathbf{i}_\mathrm{b}\mathrm{d}V_0$.

The magnetic flux density generated by bounded surface currents is given by analogical formula

$$\mathbf{B}(\mathbf{r}) = \frac{\mu_0}{4\pi}\int_{(S)} \frac{\mathbf{j}_b(\mathbf{r}_0)\times(\mathbf{r}-\mathbf{r}_0)}{|\mathbf{r}-\mathbf{r}_0|^3}\,\mathrm{d}S_0 \tag{7}$$

where symbol (S) means the total surface of permanent magnet. Application of the field and material position vectors is the same as in the previous case, Eq. (6). In our approximation of uniform magnetization, Eq. (6) is omitted and Eq. (7) considerably reduces. Details are not given here; see Ref. [5], for instance.

Elementary magnetic force, by which the magnetic field of flux density $\mathbf{B}$ acts on volume current element $\mathbf{i}\mathrm{d}V$ is given by the Lorentz Law

$$\mathrm{d}\mathbf{F} = (\mathbf{i} \times \mathbf{B})\,\mathrm{d}V. \tag{8}$$

Again the symbol x is used for vector product. For application on permanent magnets in general, the elementary force is due to both the surface and volume bounded currents. In Eq. (8) their sum should be used, one term contains the volume element $\mathrm{d}V$ and volume current density $\mathbf{i}_\mathrm{b}$ while the other consists of the surface element $\mathrm{d}S$ and corresponding surface density $\mathbf{j}_\mathrm{b}$. Analogically, the flux density $\mathbf{B}$ is eq. (8) is due by both the volume and surface bounded currents. Final formula is quite complicated.

We limit to our assumption that only bounded surface current exist. Then the Equation (8) can be written in the form

$$\mathbf{F} = \frac{\mu_0}{4\pi}\int_{(S)} \mathbf{j}_b(\mathbf{r})\times\left(\int_{(S)} \frac{\mathbf{j}_b(\mathbf{r}_0)\times(\mathbf{r}-\mathbf{r}_0)}{|\mathbf{r}-\mathbf{r}_0|^3}\,\mathrm{d}S_0\right)\mathrm{d}S \tag{9}$$

where $\mathrm{d}S_0$ is the surface element at material position vector $\mathbf{r}_0$, where exciting surface current $\mathbf{j}_\mathrm{b}(\mathbf{r}_0)$ flows. Analogically $\mathrm{d}S$ is the surface element at field position vector $\mathbf{r}$, where the elementary force acts on surface current $\mathbf{j}_\mathrm{b}(\mathbf{r})$ flowing in this element. Analogical equations as Eq. (9) can be written, if only volume currents are considered.

In the case of ring magnets both the inner and outer surfaces must be considered, as in Fig. 1. Practically important is the case, when surface currents are replaced by line currents as their sum. Then the integration is over circle instead of cylindrical surface and computation time is reduced at least by one order.

3. Experiment

The model verification is not possible without complete, precise and extensive experiments. Therefore, experiments were realized for both the measurement of the spatial distribution of magnetic flux density and the determination of the repulsive force dependence on the distance between magnets. Only basic information is given here, see Fig. 2, details can be found elsewhere [6].

3.1. Magnetic field measurement

The spatial distribution of magnetic field measurement was fully automated. The one-dimensional (1D) Hall probe was used for the flux density components measurement. The block scheme of realized measurement apparatus is in Fig. 2, left hand part. The concept of such a system can be divided into two parts: mechanical and electronic ones. The electronic part ensures the control of Hall probe motion and the digital processing of its analogue output. Details can be found in Ref. [5], for instance.

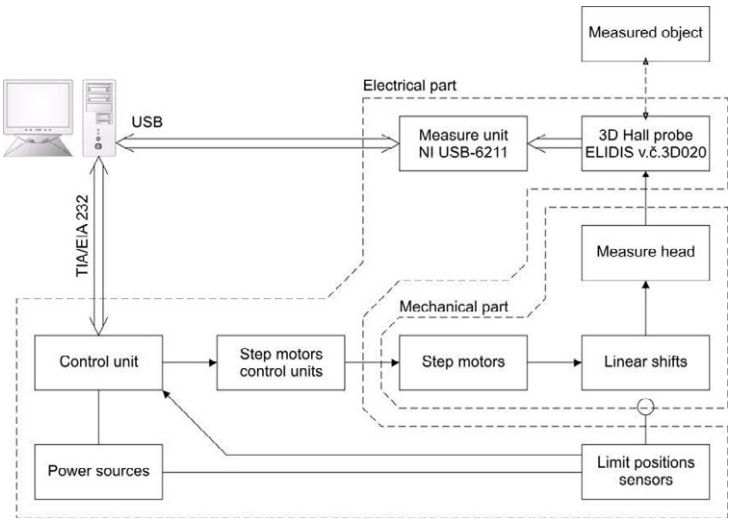

Fig. 2. Measuring systems. Block scheme of the automated apparatus for magnetic field measurement (left) and detail of the laboratory breaker (right).

The mechanical part contains separate step motor controller that drives each step motor. These units are connected to control logic processor, which translates supervising commands sent from control personal computer (PC) via universal series bus (USB) interface to electrical signals. Control unit utilizes reduced set of standard commands of system for control of physical instrument (SCPI) together with system specialized ones, which are in SCPI compliance.

Measurement, as well as position control, is done by user program at PC side. We use the MATLAB environment thanks to its simplicity and abilities of easy data processing. We have prepared fully object-oriented classes for position and motion control, data transfer via available interfaces and for data processing. It allows saving of motion history, reverting of improper steps, home setting, and independent position and speed parameters settings for each axis and online data visualization, for example.

Measurement errors are of two types: errors in probe position (mechanical errors) and errors in Hall voltage (electrical errors). Reduction of mechanical errors is made by results processing, which is reported later in the section Results. The measurement of Hall voltage exhibits a high precision. Systematic errors are due to the vibrations of mechanical parts of apparatus. After the probe reaches required position, it was necessary to wait several seconds in order the vibrations are dumped. This necessary delay results in long time of complete measurement. Measurement of about 3000 points needs about 7 hours. Parameters of the apparatus should not change during this time period.

3.2. Repulsive force measurement

The repulsive force is measured on laboratory breaker. Details are shown in the photograph at right hand part of Fig. 2. The position and force are measured by own machine software. Main problem is to get exact distance between magnets. The distance is derived from the magnet contact position. The motion continues after the contact. Since the repulsive force increases rapidly after contact, the contact position can be found from the rapid change of the slope in the measured curve. In order to reduce errors the measurement was repeated at least 10 times.

The measurement of repulsive force was used because of its simplicity. There are no problems with magnet holder. The measurement of attractive force is possible in principle and the results should be the same, if we change the force sign. Important advantage is in the precise determination of contact position. The force is zero in contact point and then changes its sign. On the other hand, the realization of magnet holder is a complicated technical task.

4. Results

All the tests were performed on several magnets made from material Fe-Nd-B, N32, Zn coated and of ring shape. Its main parameters are given in Table 1.

Measuring points and typical 3D graph of measured flux density are in Fig. 3. The net constant is 0.5 mm; therefore the net is dense enough. The magnet sides are shown in the grid. Three samples were carefully measured with the goal to show experimental and material errors. The measurement was made in only one plane, since it is time consuming. The result shown in Fig. 3 needs 7 hours.

Table 1. Basic magnet parameters

Parameter	Symbol	Value	Unit
Inner diameter	d	13.5	mm
Outer diameter	D	24	mm
Height (thickness)	h	5	mm
Magnetic flux density on magnet surface	B_r	1.15	T

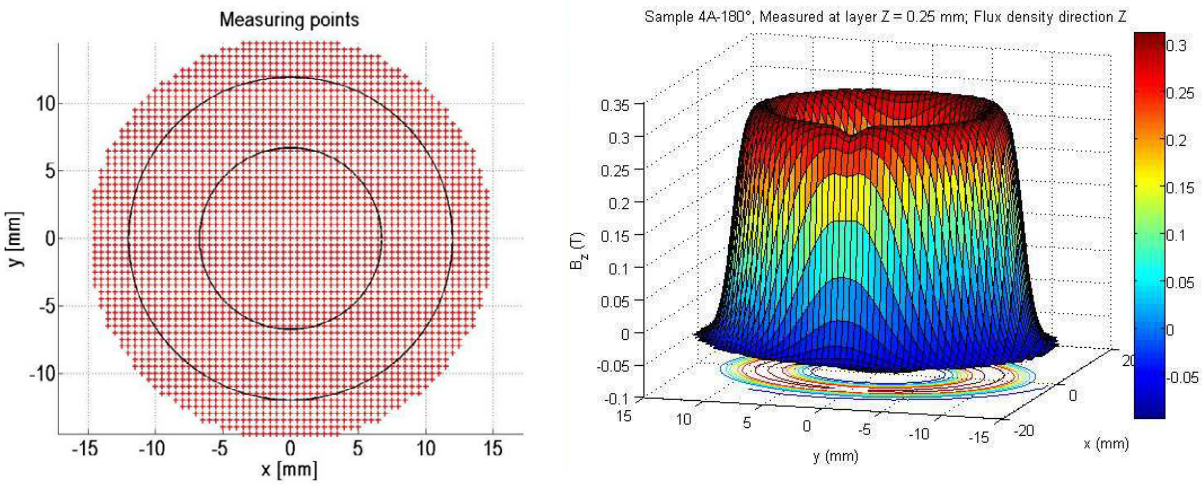

Fig. 3. Grid of measuring points (left hand side) and typical experimental result in the form of 3D graph (right hand side).

The experiments were performed with the goal to get maximum information about magnets with respect to their practical use in the analysis and design of magnetic spring. One of limitation of their use in the spring is material errors that are of two types: The difference in magnetization (and total field) of individual samples and the no uniformity of magnetization in the sample alone. Together with material errors the experimental ones exist and it is difficult to distinguish one another.

In order to get material errors, experimental ones must be reduced. Main experimental errors are:

1. The sensing element dimensions and its exact position to probe geometry.
2. The uncertainty in the of probe sensor element position above magnet surface and deviation from the expected parallel probe moving along the surface.
3. The deviation of grid centre in Fig. 3 (that determines probe position) from exact geometrical centre of the ring.

Their reduction was made in two steps: in experimental data processing and by their simulation. Processing of experimental data reduces big visible errors, while the simulation allows fine data refinement. As an example the centre shift of 0.5 mm can be found from data, but its refinement to 0.1 mm or less can be made by simulation. Therefore, we limit to experimental error simulation here, which is also one of important applications of the proposed model.

4.1. Experimental errors simulation

In order to utilize as many experimental data as possible, the simulation was made by the use of two basic geometries: lines or semi-lines going through the magnet centre and circles concentric with ring centre. Possible lines or semi-lines are sketched in Fig. 4 left hand part. The circles actually used are in the right hand part of Fig. 4. In the second case the measuring points are omitted in order to improve circle visibility. The data in these geometrical objects are obtained by interpolation of experimental data using standard procedures of MATLAB. For the perfect magnet and errorless experiment the curves for lines or semi-lines are identical and the magnetic flux density on the concentric circles should be constant. The deviation from the ideal case allows judging the material and experimental errors.

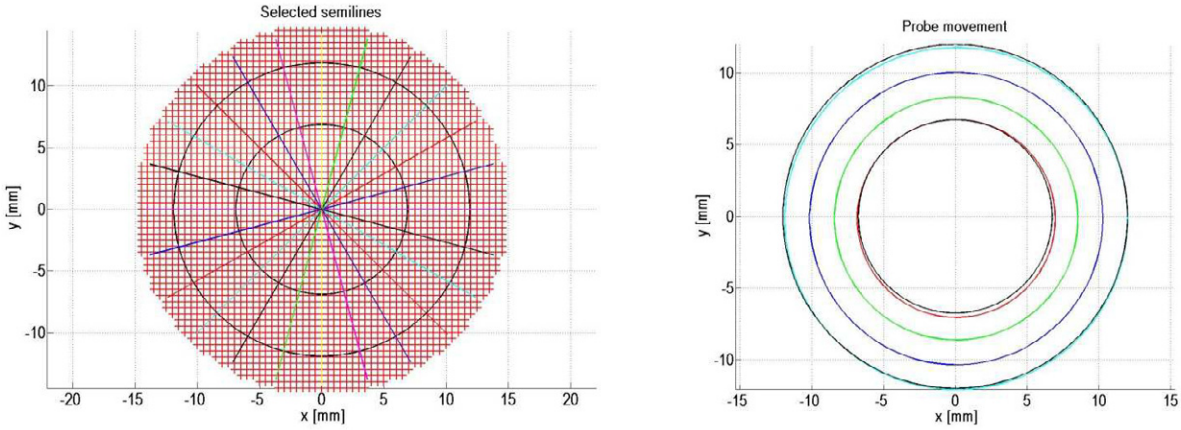

Fig. 4. Selected experimental points and their interpolation for comparison of theory and experiment: Lines or semi-lines (left), circles (right)

The effect of grid shift is shown in Fig. 5, left hand part. Only two parametric curves from the model are shown for selected experimental line of an angle of 60° in Fig. 4, left. The shift shown in Fig. 5, left, is along *X* axis. For used angle it is a half of this value. Nevertheless, its effect is well visible. The magnet vertical faces are sketched in the Fig. 5.

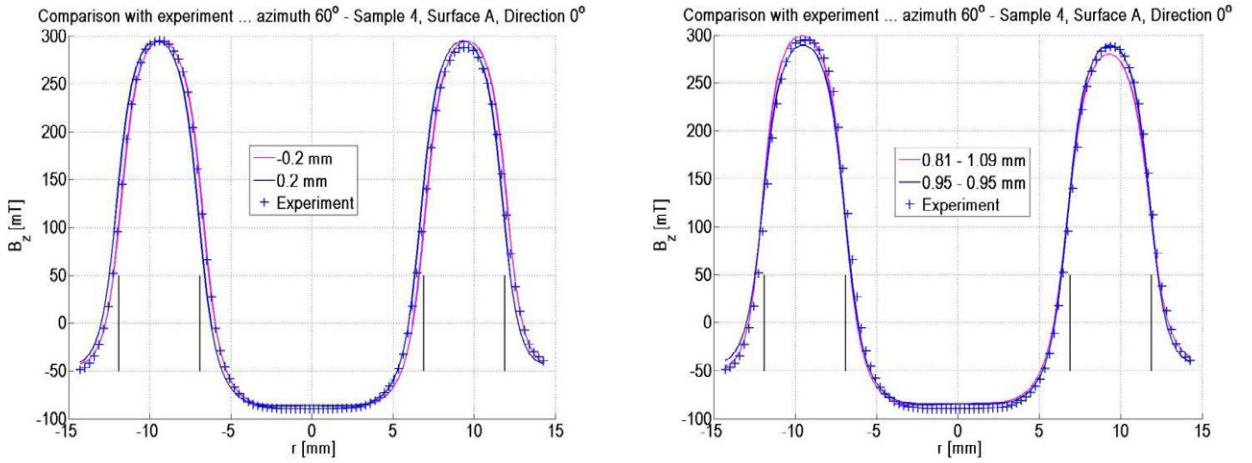

Fig. 5. Simulation of the grid centre shift (left hand side) and no parallel probe motion (right hand side) for lines going through the magnet centre

The effect of nonparallel probe motion is in Fig. 5, right hand part. Again the same experimental line is used and only two parametric curves are used. The parameters consist of two parts. They describe the probe reference position above the surface at starting and finishing point, respectively. The second curve is for the exact parallel probe motion.

The difference between origin shift and nonparallel probe motion is evident from Fig. 5. The origin shift moves the curve horizontally and its symmetry is saved. The nonparallel probe motion increases one peak and decreases the second one,

curve symmetry is missing, but there is no horizontal shift. Only vertical shift is possible, if both the parameters have the same increment.

By the selection of origin shift and probe motion parameters we can compare the agreement between theory and experiment. The goal is to get the best fit. Our approach uses the method of trials and errors. Results in Fig. 5 conform that the best fit is almost reached. The parameters have the meaning of systematic experimental errors. We can say that the agreement between model and experiment is good.

The results of simulation for the circles are in Fig. 6. The left hand part presents the effect of the origin shift. The effect is strong, but it should be mentioned that we consider the worst case, the circle close to magnet vertical face, where the flux density changes very rapidly, see Fig. 5. Unfortunately, the effect of nonparallel probe motion is almost the same. For the circles, there is only a little possibility for forecasting, in comparison with lines, where the effects are well distinguished. The comparison between theory and experiment for four selected circles is in Fig. 6, right hand part. The position of circles is shown in the right hand part of Fig. 4. The origin shift is included in the sketch in Fig. 4; therefore, the circles are not concentric. The parameter is the relative position of the investigated circle between inner and outer circle. In the central part the agreement is good, both the qualitative and quantitative one. Near the inner or outer circle the agreement is only qualitative.

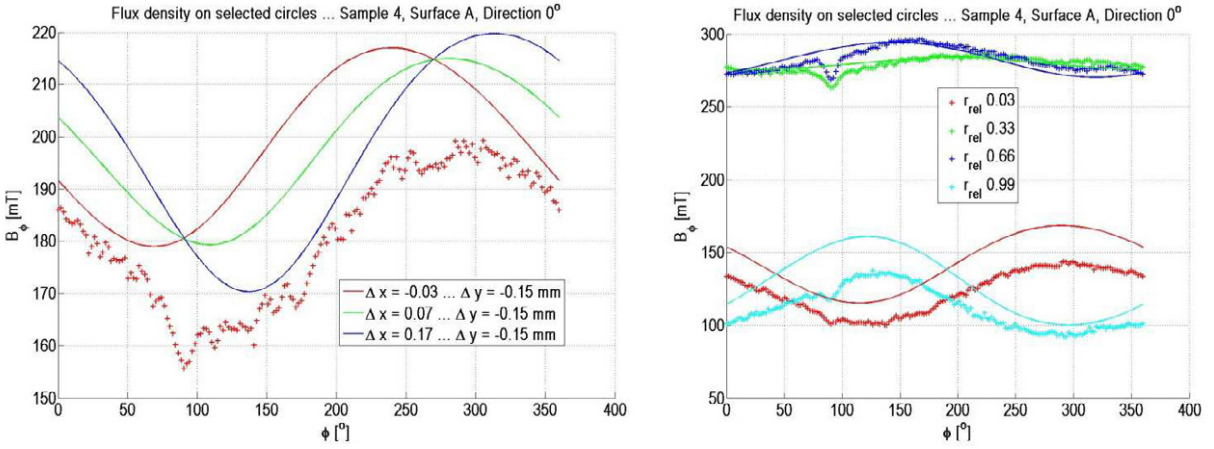

Fig. 6. Simulation of the grid centre shift for the circles (left hand side) and comparison between model and experiment for selected circles (right hand side)

The flux density shown in Fig. 6, right hand part, is not uniform; it contains both the systematic and random errors. Furthermore, the crack of the magnet ring is obvious as the abrupt change of magnetic flux density near the angle of 90°. The crack is pronounced in the central part, but it can be found near inner and outer circle too. The crack it is not noticeable visually, because it is hidden under the zinc coating.

As an example of deviation between samples and their bottom and top surfaces, Fig. 7 is presented for the rays going from the ring centre. All the experimental points for the ray of 45° with respect to the X axis are in Fig. 7, left hand part. A strong dissipation is evident. It includes both the experimental and material errors. Two curves from model are almost invisible.

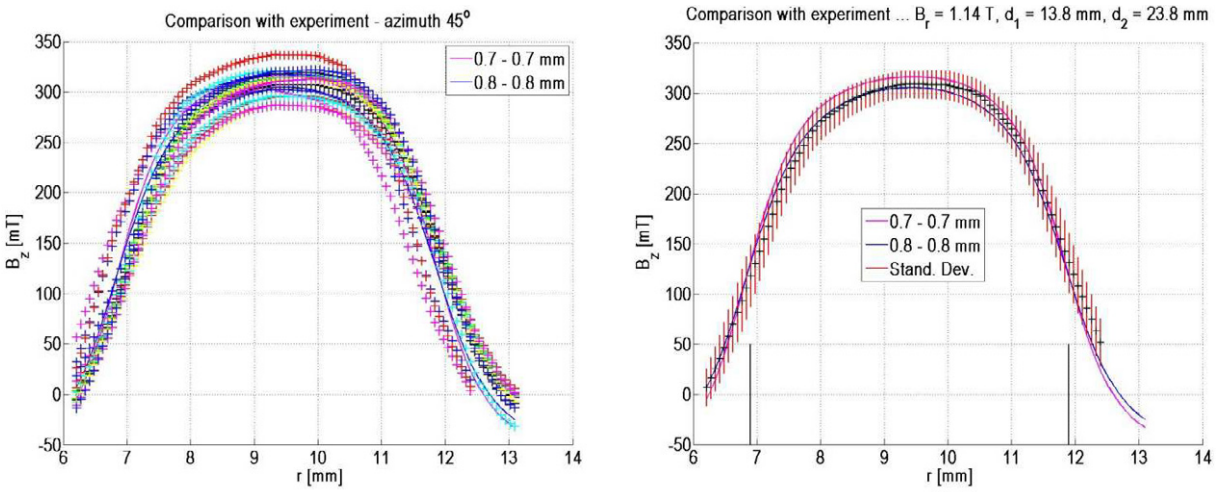

Fig. 7. Comparison between theory and experiment for all samples. Experimental results are on the left hand side and their statistical values are in the right hand side.

Statistical results are presented on the right hand side of Fig. 7. The mean value is given by points and the standard deviation by small vertical lines. The length of small vertical lines upper and down from mean values is equal the standard deviation. The deviation is almost the same for all points and it appears relatively high. The simulation curves lies within limits given by uncertainty originated both the material and experimental errors.

4.2. Repulsive force measurement

The second part of magnet investigation was the study of magnet repulsive force. The basic results for axial repulsive force are in Fig. 8, left hand part. The quantization is visible for small force values. A small asymmetry is considered, as the right hand part of Fig. 8 explains. The model was very simple. The surface bounced currents were replaced by a line current for each vertical magnet side. The value of this current is high, almost 5 kA; see Fig. 8. . The position of line current is not in the centre but a little shifted to the gap between magnets, by coefficient of 0.85 relatively to magnet thickness. Irrespective of very simple model, the agreement with experiment is good.

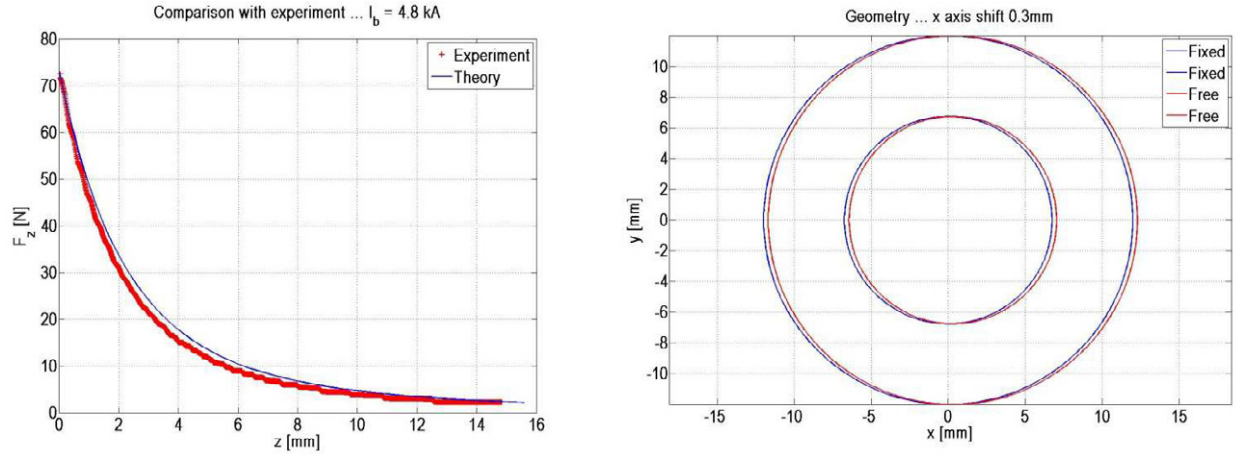

Fig. 8. Axial force – comparison between experiment and theory (left hand part) and sketch of the asymmetry (right hand part)

In general, the magnetic force does not have stable equilibrium. If the symmetry is not ensured, both the radial force and mechanic momentum appear. For the deviation of 0.1 mm from symmetric case (see Fig. 8, right hand part) the simplest

model of line currents gives the radial force and momentum in Fig. 9, left and right hand part, respectively. The radial force is not negligible.

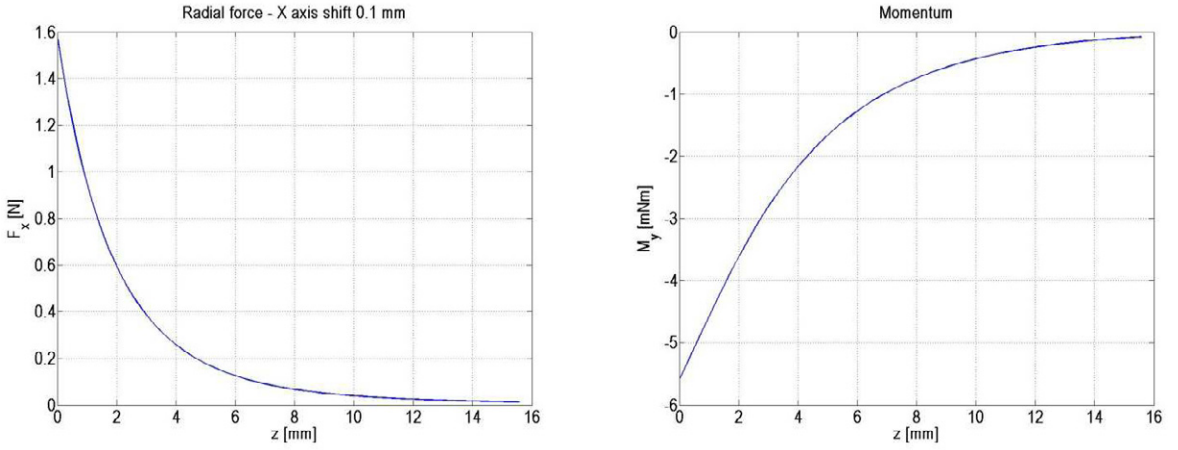

Fig. 9. Radial force (left hand part) and mechanical momentum (right hand part) for small asymmetry

5. Discussion and Conclusion

Very simple model of surface bounded currents was used. The agreement with experiment is good. Therefore, it can be used in the design of magnetic springs of prescribed parameters. Only one verification experiment is then necessary. At present time, there are some limitations, however.

The simulation can, in principle, reveal all systematic experimental errors, if enough data are to disposal. In our case we had perfect data in only one plane. Therefore, in simulation the effect of probe distance change was the same as the effect of magnetic polarization refinement. In other words, the same curves as in Fig. 5 can be obtained by increasing the magnetization and the proper decrease of the probe distance from magnet surface.

The uncertainty of systematic error parameters was the reason, why the correcting values are not reported here. In order to get correct values, more measurement are necessary, at least in other parallel planes with magnet surface. The better solution is to use planes containing the axial axis, at least the two perpendicular planes, for instance planes $x = 0$ and $y = 0$.

The same is valid for the very simple model for force calculation. It can be improved simply by the inclusion of surface bounded currents, but the time of calculations increases considerably. Thanks to good agreement with theory for axial force, we can expect that the calculations for radial force and momentum are valid. Their experimental determination is enormously difficult. Unfortunately, they plays important negative role in the actual devices.

Acknowledgements

The work was supported by the project MPOFR-TI3/047 Mechatronics of spinner machines.

References

[1] Croat, J.J., 1989. Currents status of Rapidly Solidificated Nd-Fe-B Magnets. IEEE Transactions on Magnetics 25, p 3550.
[2]Fidler, J., Tawara, Y., 1988. TEM Study of Precipitation of iron in Nd-Fe-B Magnets. IEEE Transactions on Magnetics 24, p. 170.
[3] Ruoho, S., Arkioo, A., 2008. Partial Demagnetization of Permanent Magnets in Elecrical Machines Caused by an Inclined Filed. IEEE Transactions on Magnetics 44, p. 1773.
[4] Haavisto, M., Tuomonen, S., Kankaanpaa, H., Paju M., 2010. Time Dependence of Demagnetization and Flucx Loosses Occuring in Sintered Nd-Fe-B Permannet Magnets. IEEE Transactions on Magnetics 46, p. 3582.
[5] Mikolanda, T., Kosek, M., Richter, A., 2010. Modelling and Mesaurement of Permanent Magnets. Acta Technica, 55, p. 63.
[6] Novak, M., Cernohorsky, J., Kosek, M., 2012Partial demagnetization of Fe-Nd-B permanent magnets used for magnetic spring. Proceedings of the 15th International Power Electronics and Motion Control Conference, EPE-PEMC, Novi Sad, Serbia. To be published.